Atmospheric Research 226 (2019) 240–254

Contents lists available at ScienceDirect

Atmospheric Research

journal homepage: www.elsevier.com/locate/atmosres

Decrease in light precipitation events in Huai River Eco-economic Corridor, a climate transitional zone in eastern China

Yuqing Zhang[a,b,*], Chuanming Liu[a], Qinglong You[b,c], Changchun Chen[d], Wenxin Xie[c], Zhengwei Ye[a], Xinchuan Li[a], Qiaoning He[a]

[a] School of Urban and Environmental Science, Huaiyin Normal University, Huai'an 223300, China
[b] Department of Atmospheric and Oceanic Sciences & Institute of Atmospheric Sciences, Fudan University, Shanghai 200433, China
[c] Key Laboratory of Meteorological Disaster, Ministry of Education (KLME)/Joint International Research Laboratory of Climate and Environment Change (ILCEC), Nanjing University of Information Science and Technology, Nanjing (NUIST), 210044, China
[d] School of Geographical Sciences, NUIST, 210044, China

ARTICLE INFO

Keywords:
Light precipitation events
Consecutive light precipitation
Atmospheric circulation
Huai River Eco-economic Corridor

ABSTRACT

Light precipitation events generally occur much more frequently than events of other precipitation intensities. Changes in light precipitation amounts and days (length) over time have profound implications for climate change. There is a lack of quantitative monitoring indicators or in-depth analysis techniques for atmospheric circulation mechanisms of regional light precipitation events, especially in climate transitional zones. The Huai River Eco-economic Corridor (HREC) served as a case area in this study as we assessed trends in light precipitation events and their possible atmospheric circulation mechanisms. A significant decreasing trend in the light precipitation events is observed and appears to be mainly concentrated in the lower intensities ($0.1 \leq P < 2$ mm/day). The decreasing trend is more obvious for consecutive than discrete light precipitation events. The mutation points for annual consecutive light precipitation events were found in 1977/1978, and averages in the later years of the observation period (1978–2014) fell significantly below those of the earlier period (1961–1977). Atmospheric circulation variables corresponding to the light precipitation days with intensity of 0.1–2 mm/day revealed that the decreasing trends in water vapor transport budgets, low cloud cover, and total column cloud liquid water may be the primary causes of decreased light precipitation events. The decreasing trends in light precipitation events were also likely attributable to increases in water vapor flux divergence, air temperature, and vertical velocity values.

1. Introduction

Precipitation in the land areas of the mid-latitudes of the northern hemisphere has increased at high confidence since 1951 (IPCC, 2013). Global warming has altered the spatio-temporal distribution of precipitation and consequently led to an increase in hydro-climatic extremes (Tao et al., 2016; Yu et al., 2018; Zhang et al., 2017). Many researchers have explored the characteristics of extreme hydro-climatic events including extreme precipitation events (Gao et al., 2016; Wang et al., 2017), floods (Dhana Lakshmi and Satyanarayana, 2019; Mallakpour and Villarini, 2015) and droughts (Ahmed et al., 2019; Ahmed et al., 2018; Dai, 2013), as these have significant destructive power. In today's world, extreme precipitation events in many regions are increasing on the whole (Li et al., 2016; Zhai et al., 2005). These events can affect the annual precipitation structure as they account for a disproportionately high percentage of the annual total precipitation. Light precipitation generally prevails over extreme precipitation in terms of the total proportions of daily events (Liu et al., 2011).

Light precipitation is more likely to infiltrate into soil layers than more intense precipitation; to this effect, it plays an important role in maintaining soil moisture and humidifying plants. Thus, changes in light precipitation characteristics can reflect drought conditions in many regions around the world (Qian et al., 2010). The low intensity of light precipitation events makes them more sensitive to global climate change than events of stronger intensity. Qian et al. (2007) analyzed summer precipitation events of varying intensity in China based on daily-scale data to find that light precipitation events have significantly decreased in many regions. Wen et al. (2016) applied the percentile threshold method to investigate trends in light precipitation events over the global land, and found that they have decreased over eastern China

* Corresponding author at: School of Urban and Environmental Science, Huaiyin Normal University, Huai'an 223300, China.
E-mail address: geonuist@foxmail.com (Y. Zhang).

https://doi.org/10.1016/j.atmosres.2019.04.027
Received 8 January 2019; Received in revised form 8 April 2019; Accepted 23 April 2019
Available online 25 April 2019
0169-8095/ © 2019 Elsevier B.V. All rights reserved.

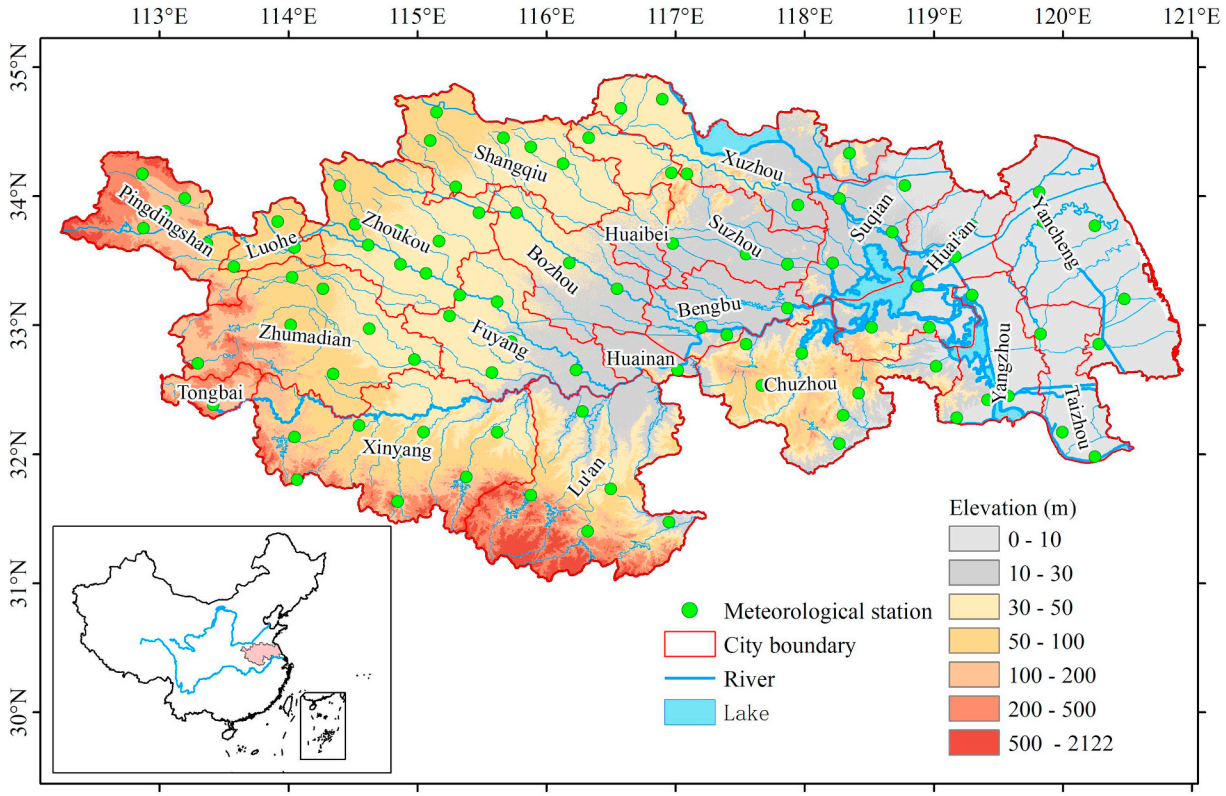

Fig. 1. Location of HREC and meteorological stations.

and northern Eurasia but increased over the U.S., Australia, and the Iberian Peninsula. Wu et al. (2017) analyzed the effects of different types of cloud cover on light precipitation events in eastern China; light precipitation events mainly occur under partly cloudy weather, which accounts for 84% of the decrease in total light precipitation events. Despite these and other valuable contributions to the literature, there are scientific issues yet to be explored. For example, there is no universal and precise definition of "light precipitation event"; the mechanism of decreasing trends in light precipitation events has yet to be fully elucidated.

Light precipitation is defined mainly based on the absolute threshold and relative threshold of a precipitation event. The absolute threshold method of light precipitation is generally considered to have intensity of 0.1 mm to 10 mm per day (Fu et al., 2008; Qian et al., 2007; Wu et al., 2015). This definition does not broadly apply in terms of regionality – the threshold range for light precipitation intensity cannot be strictly used in certain areas. Researchers have established other intensity ranges for light precipitation events, such as $0.1 \le P \le 1$ mm/day (Liu et al., 2011), $0 < P < 2$ mm/day, and $0 < P < 5$ mm/day (Qian et al., 2009). Other scholars have used the relative threshold method (fixed-percentile bins) at different stations to observe light precipitation characteristics, which partly eliminates the disadvantages of applying the same standard across different regions. For example, Wen et al. (2016) used a 50th percentile threshold to define light precipitation events at the global scale. The thresholds for most regions are around 1–5 mm/day; generally, the thresholds at lower latitudes or wetter regions are greater than those at higher latitudes or more arid regions. Relative thresholds may be quite different from region to region, and there is currently no universally accepted definition of "light precipitation event". It is necessary to determine the appropriate threshold for light precipitation events according to local conditions.

The long-term average of atmospheric circulation reanalysis data (e.g., water vapor flux and relative humidity fields) can be used to explain trends in light precipitation events (Liu et al., 2011; Qian et al., 2007). This approach reveals possible mechanisms from a climatic perspective, but holds high uncertainty as long-term average atmospheric circulation variables include non-light precipitation days. Other researchers have applied composite analysis methods to atmospheric circulation data to explore light precipitation events (Li et al., 2016; Wu et al., 2015; Yao et al., 2017). Composite analysis reveals atmospheric circulation patterns that are more likely to occur in light precipitation events, but does not explain long-term trends in such events. Researchers have also assessed trends in light precipitation events from the perspective of aerosol usage (Qian et al., 2009; Wu et al., 2016), i.e., as-affected by anthropogenic activities. However, there is little data for aerosol content at different atmospheric layers, and it is difficult to obtain precise long-term series as aerosol observation stations are sparse and have existed for a relatively short-term period. It is necessary to use atmospheric circulation patterns to explain long-term trends in light precipitation events, as the atmospheric circulation reanalysis product has large spatial coverage, long time series, abundant variables, and good data quality.

In this study, we used the Huai River Eco-economic Corridor (HREC) as an example to investigate the characteristics and atmospheric circulation mechanisms of light precipitation events. The primary goals of this study include: 1) exploring the spatio-temporal characteristics of annual light precipitation events using different precipitation intensity methods, 2) determining the characteristics of annual consecutive light precipitation events, and 3) elucidating the role of atmospheric circulation in light precipitation events by attributing certain circulation patterns to light precipitation days. The HREC is a key agricultural region, accounting for 14.4% of the total grain production in China. Its light precipitation characteristics are of vital importance to nationwide agricultural production because such precipitation supplements the soil moisture and favors crop growth. In addition, the findings presented here may provide a scientific basis for drought resistance treatments and overall water resource management in regions that share similar climatic and socio-economic characteristics with the HREC.

2. Materials and methods

2.1. Study area

The HREC is located between 112°E – 121°E and 31°N -35°N in eastern China (Fig. 1). It has an approximate area of 200,000 km^2, which represents three-quarters of the entire Huai River Basin. It lies between the Yangtze River and Yellow River, which belongs to a climate transitional zone of North and South China; this is the humid and semi-humid monsoon climate region of eastern China and a transitional zone of high and low latitudes between the country's sea and land regions. The Huai River is the main linkage (main route) in the HREC covering He'nan, Anhui, and Jiangsu provinces encompassing a total of 20 prefecture-level cities and one county-level city.

The HREC is a flagship project area for domestic regional cooperation and development (Gu and Zhang, 2016). It covers a vast plain with mountains and foothills at its western and southern reaches, where most regions have altitude below 100 m (above the mean sea level). The HREC encompasses 12.5% of China's cultivated land supporting a population of 129 million, and is thus of great socio-economic importance. The region receives annual mean precipitation of 910 mm and has an annual mean temperature of 14.5 °C. As shown in Fig. 2a, the overall distribution of precipitation decreases from southeast (~1200 mm) to northwest (~700 mm). The standard deviation distribution of annual precipitation is more consistent with that of annual mean precipitation, reaching a maximum (280 mm) in the eastern and southern parts and a minimum (180 mm) in the northwestern part of the region (Fig. 2b). Therefore, drought and flood risk in the southeastern region is higher than that in the northwestern region. In the summer, the region is controlled by the Plum Rain front (*Meiyu*) and subtropical high which make it prone to flood and drought events (Zhang et al., 2015).

2.2. Data

Daily precipitation data for 1961–2014 was provided by the National Climate Center of the China Meteorological Administration. The dataset was subjected to quality control and homogeneity testing before its release. To consider the integrity and continuity of the series, any station was removed from the study if > 31 days during 1961–2014 were missing from its data (25 stations were excluded). We ultimately included 95 surface station data spanning 1961–2014 (Fig. 1). Missing precipitation values (< 31 days during 1961–2014) for one station were replaced with values of adjacent stations.

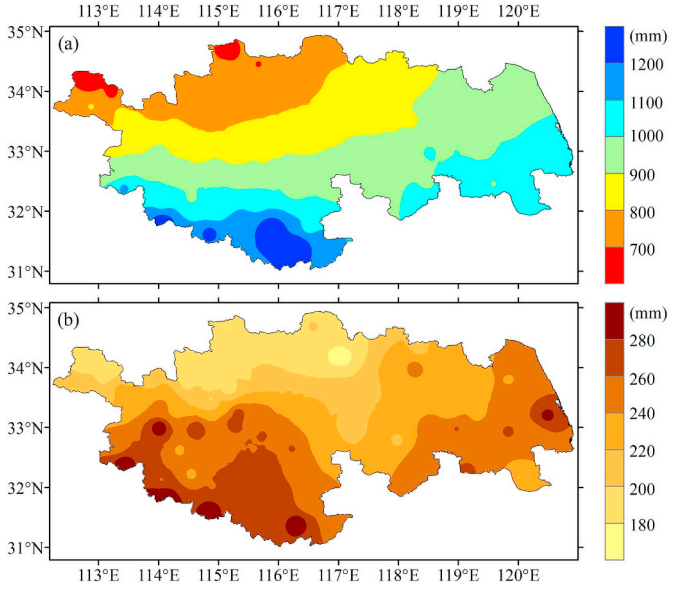

Fig. 2. Patterns of (a) annual mean precipitation and (b) one standard deviation from 1961 to 2014.

The European Center for Medium-Range Weather Forecasts (ECMWF) pilot reanalysis of the 20th-century assimilating surface observations only (ERA−20C) attempts to reconstruct the weather history between years 1900 and 2010, using a 10-member ensemble of 24-h 4D-Var analyses (http://apps.ecmwf.int/datasets/data/era20c-daily/levtype=pl/type=an/) (Poli et al., 2013). In order to be consistent with the time series of precipitation observations (1961–2014), we finally selected water vapor flux, low cloud cover, total column cloud liquid water, air temperature, and vertical velocity fields from 1961 to 2010. The data has a 0.5° × 0.5° horizontal resolution and 15 vertical pressure layer (1000, 950, 900, 850, 800, 750, 700, 650, 600, 550, 500, 450, 400, 350, 300 hPa). The original temporal resolution of the dataset is 8 times per day (3-h product). The daily means of these variables were computed to determine the atmospheric circulation mechanism of light precipitation trends.

2.3. Methods

2.3.1. Definition of light precipitation events

A precipitation event is generally defined as ≥0.1 mm/day (Liu et al., 2011; Zhai et al., 1999). We adopted the 0.1 ≤ P < 10 mm/day definition for light precipitation event (Qian et al., 2007; Wu et al., 2015). This criterion can be found in the standards of the China Meteorological Administration, which provides five grades of intensity for daily precipitation rates: light (0.1 ≤ P < 10 mm/day), moderate (10 ≤ P < 25 mm/day), large (25 ≤ P < 50 mm/day), heavy (50 ≤ P < 100 mm/day), and extreme (≥100 mm/day).

To further analyze the light precipitation events, we split them into five grades of intensity: grade 1 (G1) (0.1 ≤ P < 2 mm/day), G2 (2 ≤ P < 4 mm/day), G3 (4 ≤ P < 6 mm/day), G4 (6 ≤ P < 8 mm/day), and G5 (8 ≤ P < 10 mm/day). To examine the persistence of the light precipitation, we defined a period ≥3 consecutive days of light precipitation as a "consecutive" event. We established a consecutive light precipitation magnitude index (CLPMI) which takes into account both the magnitude and duration of one such event. CLPMI can be calculated for one event at a given station as follows:

$$CLPMI = G_1 \cdot D_1 + G_2 \cdot D_2 + G_3 \cdot D_3 + G_4 \cdot D_4 + G_5 \cdot D_5 \quad (1)$$

where G denotes the specific grade of light precipitation and D is the number of days of light precipitation at said grade. For example, a light precipitation event lasting for 5 days with precipitation amounts of 0.2, 1.3, 2.4, 5.6, and 8.1 mm, respectively, has CLPMI of $G_1(1)\cdot D_1(2) + G_2(2)\cdot D_2(1) + G_3(3)\cdot D_3(1) + G_4(4)\cdot D_4(0) + G_5(5)\cdot D_5(1) = 1\cdot 2 + 2\cdot 1 + 3\cdot 1 + 4\cdot 0 + 5\cdot 1 = 12$.

2.3.2. Cramér-von Mises test

We used Cramér-von Mises (CvM) change point detection to evaluate temporal changes in consecutive light precipitation events (Holmes et al., 2013). Mazdiyasni and Aghakouchak (2015) found that the CvM is more sensitive to potential changes in climate time series than the Mann-kendall test. Sharma and Mujumdar (2017) used the CvM method to analyze the mutations of the concurrent meteorological droughts and heat waves in India from 1951 to 2010, and concluded that the concurrent events were significant mutations occurred in 1980. The CvM approach detects mutation points by comparing two subsamples of the original time series.

$$\widehat{F}_s(x) = \frac{1}{\tau}\sum_{i=1}^{\tau} I\,(x_i \le x) \quad (2)$$

$$\widehat{F}_t(x) = \frac{1}{n-\tau}\sum_{i=\tau+1}^{\tau} I\,(x_i \le x) \quad (3)$$

where $\widehat{F}_s(x)$ and $\widehat{F}_t(x)$ are the empirical cumulative distribution

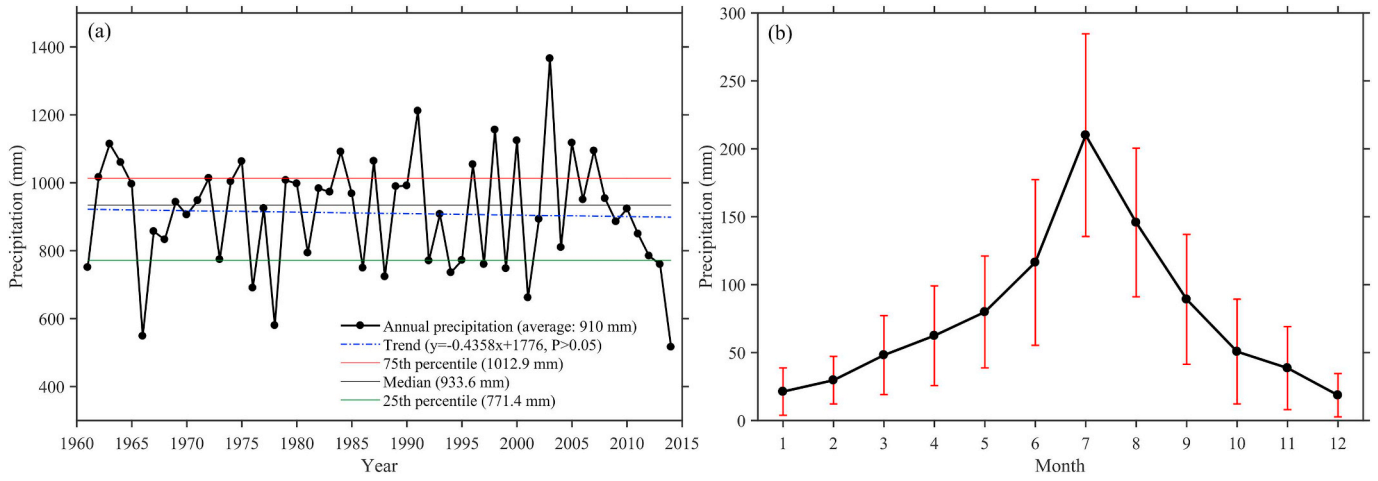

Fig. 3. Annual series of (a) total precipitation and (b) climatology of monthly mean precipitation over HREC from 1961 to 2014. Error bars represent one standard deviation of interannual variation of precipitation in each month.

function of the two subsamples. I represents the indicator function, n is the sample size, and the terms $1/\tau$ and $1/(n-\tau)$ denote adjustment factors for the length of each subsample. Divergence between the empirical distributions in the CvM test statistic can be measured as follows:

$$W_{\tau,n} = \int_{-\infty}^{\infty} |\widehat{F}_s(x) - \widehat{F}_t(x)|^2 dF(x) \tag{4}$$

where $W_{\tau,n}$ can be calculated as the square of the mean distance between the empirical distributions (Mazdiyasni and Aghakouchak, 2015).

$$W_{\tau,n} = \sum_{i=1}^{n} \int_{-\infty}^{\infty} |\widehat{F}_s(x_i) - \widehat{F}_t(x_i)|^2 \tag{5}$$

A larger $W_{\tau,n}$ value indicates greater change in the cumulative distribution. The null hypothesis is rejected if at an unspecified point τ, $\widehat{F}_s(x)$ and $\widehat{F}_t(x)$ come from statistically different distributions.

2.3.3. Water vapor flux

The vertically integrated water vapor flux over the HREC can be written as the following forms (Trenberth, 1991):

$$Q_u = -\frac{1}{g}\int_{P_s}^{P_t} qudp \tag{6}$$

$$Q_v = -\frac{1}{g}\int_{P_s}^{P_t} qvdp \tag{7}$$

where g, q, u, v, and p are gravitational acceleration, specific humidity, zonal wind, meridional wind, and pressure, respectively; P_s and P_t are the surface and top pressure. The water vapor flux is integrated from surface pressure to 300 hPa (P_t) as there is negligible water vapor above 300 hPa (Zhou, 2003).

We used the following equations to quantitatively calculate water vapor transport across the boundaries of the HREC (Lin et al., 2016):

$$F_u = \int Q_u a d\phi \tag{8}$$

$$F_v = \int Q_v a \cos\phi d\lambda \tag{9}$$

and

$$D_s = \sum (F_u, F_v) \tag{10}$$

where a, ϕ, and λ represent the earth's radius, latitude, and longitude, respectively; F_u, F_v, and D_s denote zonal, meridional, and regional net water vapor balance, respectively.

2.3.4. Linear regression

Linear regression was applied to calculate the light precipitation trends and to explore the possible linkages between atmospheric variables and light precipitation events. The equation is (Duan and Wu, 2008):

$$y_i = a + bx_i \tag{11}$$

where i is the time step (i = 1, 2, 3, …, n); a and b are the regression constant and linear regression coefficient, respectively, which can be estimated via the least squares method:

$$b = \frac{\sum_{i=1}^{n} y_i x_i - \frac{1}{n}\left(\sum_{i=1}^{n} y_i\right)\left(\sum_{i=1}^{n} x_i\right)}{\sum_{i=1}^{n} x_i^2 - \frac{1}{n}\left(\sum_{i=1}^{n} x_i\right)^2} \tag{12}$$

$$a = \bar{y} - b\bar{x}, \text{ where } \bar{y} = \frac{1}{n}\sum_{i=1}^{n} y_i, \bar{x} = \frac{1}{n}\sum_{i=1}^{n} x_i \tag{13}$$

When calculating the linear trend of a specific variable (e.g., light precipitation amounts and days), y is the specific variable and x is the annual time series. When exploring the light precipitation event mechanism, y is the atmospheric circulation variable and x is the light precipitation event.

3. Results

3.1. Annual precipitation characteristics

Annual precipitation does not explicitly exhibit significant linear trends in the HREC from 1961 to 2014 (Fig. 3), but does have clear-cut fluctuations. Annual precipitation in most years is outside the range of 25th–75th percentiles, indicating that the risk of drought and flood is significant. Extraordinary droughts occurred in the years 1966, 1978, 1988, 1994, 1999, 2001, and 2014, and extraordinary floods occurred in 1991, 2003, 2005, and 2007. Summer season (June, July, and August) precipitation is the largest (average over 100 mm in each month) and has the widest variability, indicating that summer months are most prone to flood and drought events.

The distribution of annual precipitation days shows a north-south gradient (Fig. 4a) decreasing from > 125 days in the south to < 85 days in the north. Most stations exhibited a significant decrease in annual precipitation days. About half of the stations show trends in the range of −10 to −3 days/decade. Annual mean precipitation days averaged over all stations in the HREC were 103.9 days (Fig. 4b). The entire

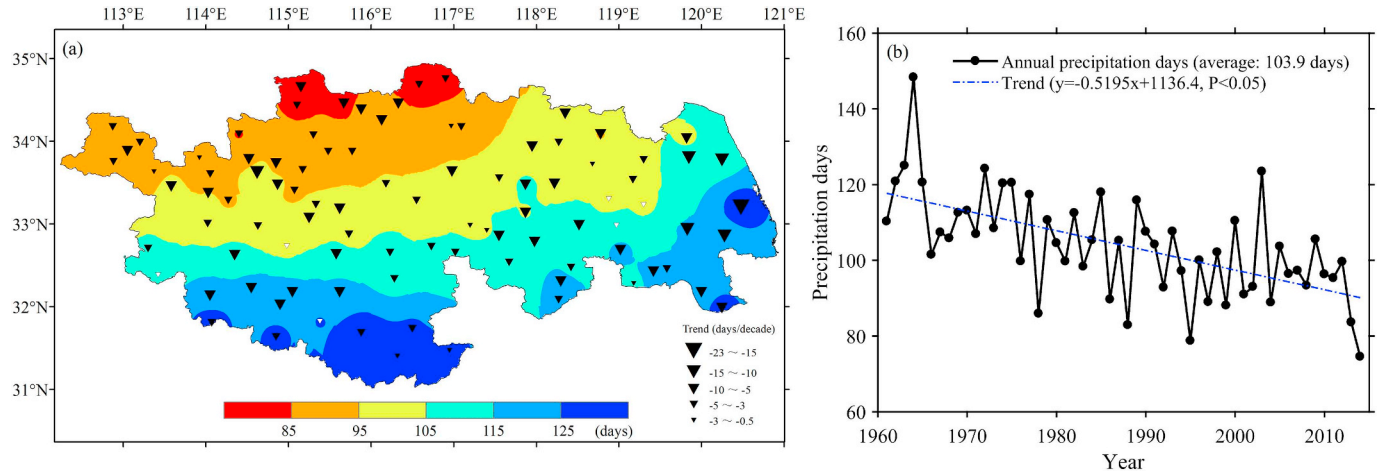

Fig. 4. Spatial distribution of (a) precipitation days and linear trends, and (b) annual precipitation days averaged over HREC from 1961 to 2014. Upward and downward triangles denote increase and decrease trends, respectively; solid triangles represent linear trends reaching 0.05 significance level.

HREC showed a significant decreasing trend of −5.2 days/decade in annual precipitation days (Fig. 4b), but there was no significant trend in annual precipitation amount from 1961 to 2014 (Fig. 3a).

3.2. Spatial and temporal characteristics of annual light precipitation

This study focuses on the characteristics of annual light precipitation events. Fig. 5 shows the characteristics of light precipitation amounts and days over the observation period in the HREC. The annual mean light precipitation decreased from > 260 mm in the south to < 160 mm in the north (Fig. 5a) with distinct zonal distribution features. Annual light precipitation showed a downward trend in most stations. Only the stations in the northwestern parts of region passed the 0.05 significance test (Fig. 5a). We found that spatial changes in light precipitation days were consistent with the precipitation amounts (Fig. 5b), implying that light precipitation events in the southern part of the region are more intense than in northern parts of the region. Southern parts of the region saw up to 95 days of light precipitation while there relatively low values (< 70 days) are concentrated in the northern parts of the region. Almost all stations show a significant decrease in annual precipitation days over the observation period, most at a rate of −11 to −2 days/decade. Annual mean light precipitation and days are 193.4 mm and 78.7 days (Fig. 5c). On the whole, light precipitation in the HREC decreased about 4.8 mm/decade in the 54-year period we observed. Light precipitation days decrease to greater extent than precipitation amounts at a rate of around −5.1 days/decade.

As shown in Fig. 5d, light precipitation encompasses about 21–27% of the total precipitation amounts in the study area. There was a weak decreasing trend during 1961–2014, only a few stations in northwestern parts of the region showed a significant downward trend at the rate of −2.2% to −1%/decade. However, the light precipitation day proportion decreased significantly from −2.9% to −1%/decade at most stations (Fig. 5e). Although light precipitation accounts for only 22.5% of the total precipitation amount, the number of light precipitation day accounts for 75.7% of total precipitation days (Fig. 5f). In other words, most precipitation events in the HREC are light. The

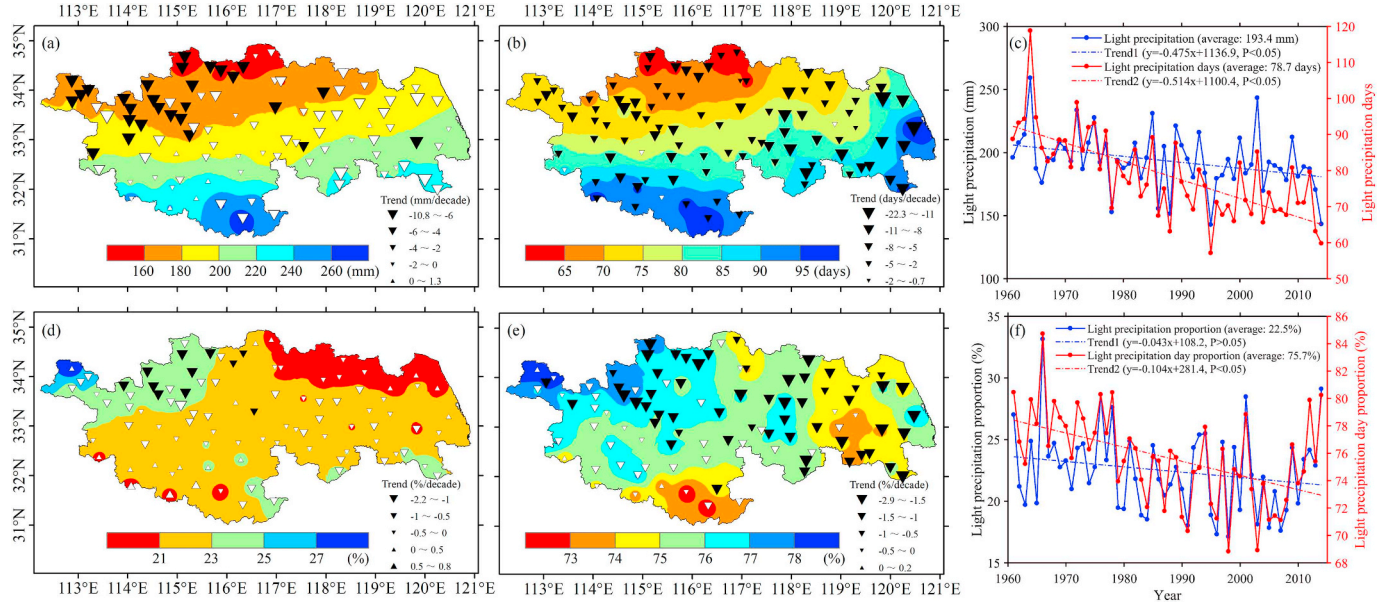

Fig. 5. Spatial and temporal characteristics of light precipitation events. (a) Light precipitation amounts, (b) light precipitation days, (c) annual changes, (d) light precipitation amount proportion in total precipitation, (e) light precipitation day proportion in total precipitation, and (f) annual proportions in total precipitation amounts and days. Upward and downward triangles denote increase and decrease trends, respectively; solid triangles represent linear trends reaching 0.05 significance level.

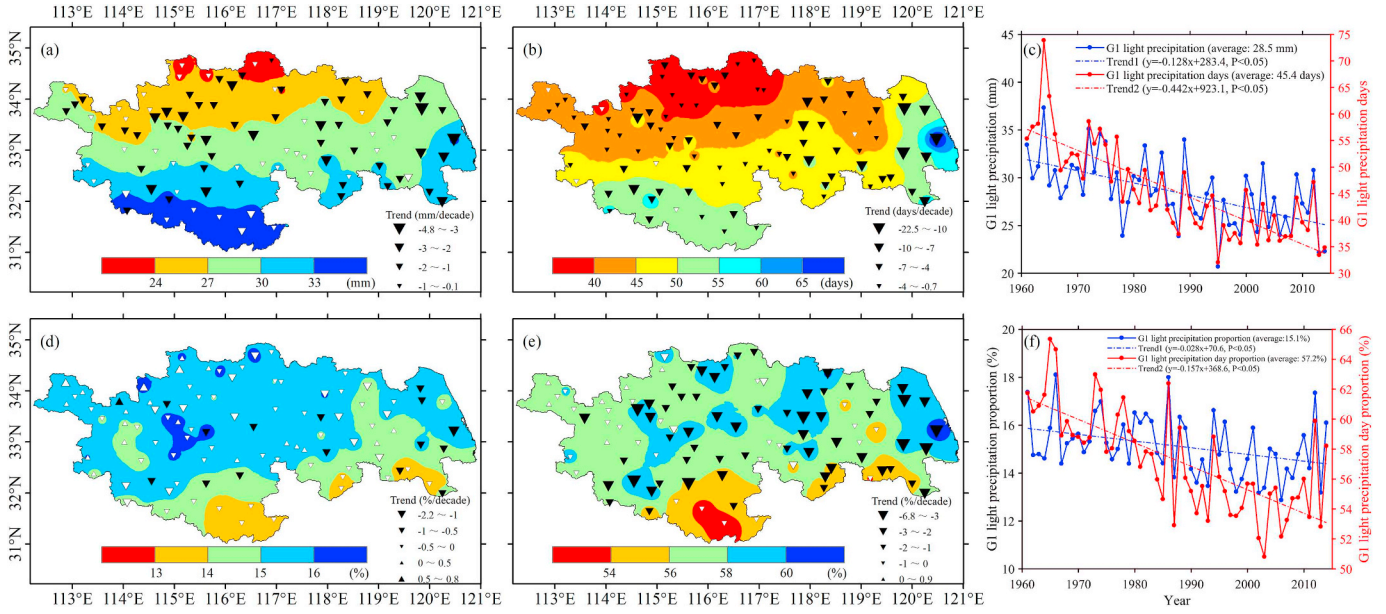

Fig. 6. Spatial and temporal characteristics of G1 light precipitation events. (a) G1 light precipitation amounts, (b) G1 light precipitation days, (c) annual changes, (d) G1 proportion in total light precipitation amount, (e) G1 day proportion in total light precipitation days, and (f) annual proportions in total light precipitation amounts and days. Upward and downward triangles denote increase and decrease trends, respectively; solid triangles represent linear trends reaching 0.05 significance level.

proportion of light precipitation days decreased to greater extent than the light precipitation amount decreased over the observation period.

As mentioned above, we divided the light precipitation events into five intensity grades using equal interval division to assess whether any decreasing trends were uniform. The grades include G1 ($0.1 \le P < 2$ mm/day), G2 ($2 \le P < 4$ mm/day), G3 ($4 \le P < 6$ mm/day), G4 ($6 \le P < 8$ mm/day), and G5 ($8 \le P < 10$ mm/day). The amount of G1 light precipitation shows obvious zonal distribution characteristics (Fig. 6a), with high values in the south (> 33 mm) and the low values in the north (< 24 mm). The G1 precipitation amount in more than half of the stations decreased significantly over the observation period. The distribution of G1 light precipitation days is similar to that of precipitation amounts – more stations show a significant downward trend in terms of days compared to amounts (Fig. 6b). As shown in Fig. 6c, annual mean G1 light precipitation amounts and days are 28.5 mm and 45.4 days, respectively. Both the G2 light precipitation amounts and days showed a significant downward trend at decreasing rates of −1.3 mm/decade and − 4.4 days/decade, respectively.

The proportion of G1 light precipitation to total light precipitation amount ranges from about 13–16% (Fig. 6d), while G1 days account for 54–60% of the total light precipitation days (Fig. 6e). G1 light precipitation amount proportion trended downward at most stations, but only about 15% of the stations showed decreasing trends at the 0.05 significance level (Fig. 6d). The proportion of G1 days in the total light precipitation days decreased significantly at most stations (Fig. 6e). According to Fig. 6f, the proportions of annual mean G1 light precipitation amounts and days are 15.1% and 57.2%, respectively. This implies that precipitation events with intensity between 0.1 and 2 mm/day account for more than half of the total light precipitation events ($0.1 \le P < 10$ mm/day) in the study region, despite the small proportion of total light precipitation amount. Overall, the proportion of G1 light precipitation days decreased to greater extent than the precipitation amounts at a rate of around −1.6%/decade.

As shown in Fig. 7a, there is an obvious south-north transition in the spatial distribution of G2 light precipitation amounts on the annual mean. Maximum G2 light precipitation amounts (> 50 mm) appear in the southern parts with a decline gradient to the northern parts (< 35 mm) of the region. Approximately 15% of stations exhibit a significant downward trend and these stations are primarily located in the northwestern part of the region (Fig. 7a). The distribution of G2 light precipitation days is in line with the distribution of precipitation amounts – the more G2 precipitation the region receives, the more G2 days it experiences (Fig. 7b). As shown in Fig. 7c, the annual mean G2 light precipitation amounts and days are 39.7 mm and 14 days, respectively. Both the G2 light precipitation amounts and days showed a significant downward trend at decreasing rates of −0.9 mm/decade and − 0.3 days/decade, respectively. These decreasing trends were less intense than those of G1.

Fig. 7d shows a slight upward trend in the proportion of G2 light precipitation amount but a significant increasing trend in the proportion of G2 days (Fig. 7e). The proportion of G2 light precipitation amounts fall roughly from 20% to 22% (Fig. 7d), with trends partially upward and downward but almost none passing the 0.05 significance level. As shown in Fig. 7e, the proportion of G2 light precipitation days in most areas ranges from 16% to 19% of the total with similar spatial distribution characteristics to the amount of G2 light precipitation. About half of the stations show a significant upward trend in the proportion of G2 light precipitation days. According to Fig. 7f, the proportions of annual mean G2 light precipitation amounts and days are 20.8% and 18%, respectively. Although the proportion of G2 annual mean light precipitation amount is slightly greater than that of G1 (15.1% in G1 and 20.8% in G2), the proportion of G2 light precipitation days is much lower than that of G1 (57.2% in G1 and 18% in G2). There are more significant increases in the proportion of G2 light precipitation amounts than days (Fig. 7f).

The spatial distribution characteristics of annual mean G3 light precipitation amounts and days are similar to those of G2 (high values in the south and low values in the north), but only a few stations show any significant downward trend (Fig. 8a and b). Stations with significant decreasing trends are mainly concentrated in the northwestern parts of the region. The annual changes in G3 light precipitation amounts and days across the region are relatively consistent; both slope gently downward at rates of −0.8 mm/decade and − 0.2 days/decade, respectively (Fig. 8c). The amount of G3 light precipitation is basically equal to G2, but there were only 8 days of G3 (about 60% of G2).

The proportions of G3 light precipitation amounts showed regional differences (Fig. 8d). Only one station in the western part of the region showed a significant downward trend; two stations in the eastern parts

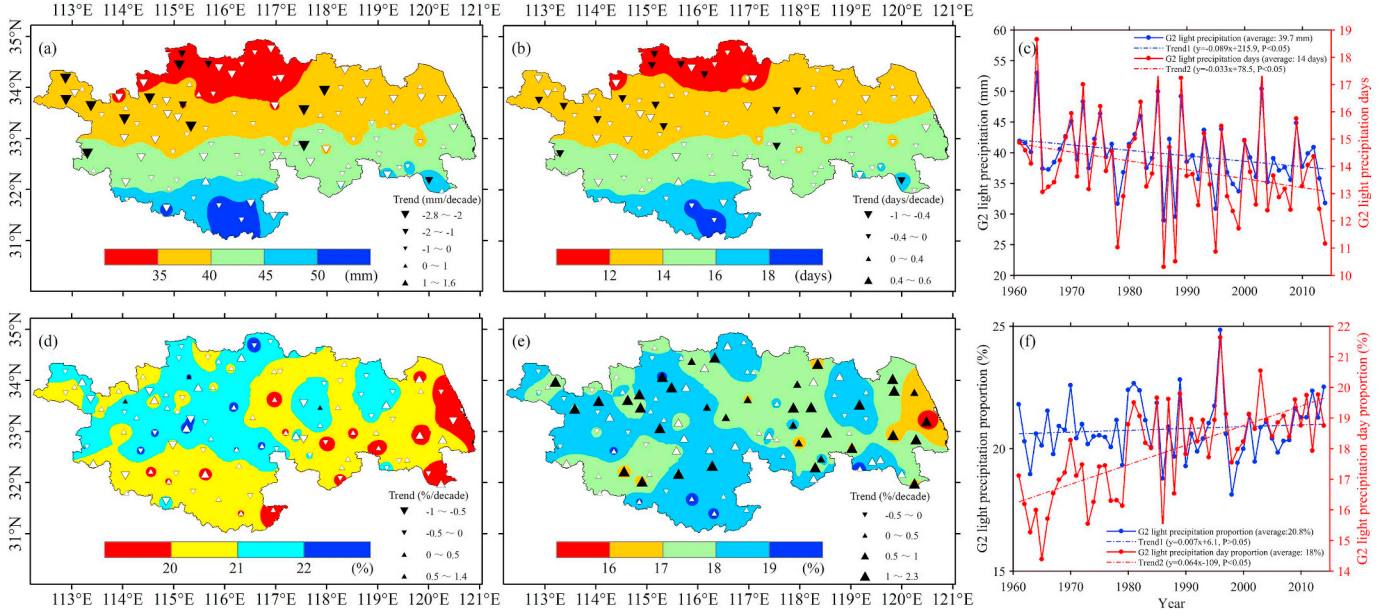

Fig. 7. The same as Fig. 6, but for G2 light precipitation events.

of the region showed significant upward trends. In fact, about half of the stations in the proportion of G3 light precipitation days showed significant upward trends (Fig. 8e). Increases in G3 light precipitation days across the region are more obvious than the changes in amount (Fig. 8f). The higher values are concentrated in years 1990–2010. The annual average proportion of G3 amount is generally equal to that of G2, but there are fewer G3 days than G2 (as low as 11% in the annual mean of G3 proportions).

The spatial distribution of the annual mean G4 amounts has an obvious south-north gradient, decreasing from > 55 mm in the south to < 35 mm in the north (Fig. 9a). Most stations exhibit a slight downward trend in G4 amounts, but only a few stations in the northwestern parts of the region pass the 0.05 significance level. The distribution of annual mean G4 light precipitation days is similar to that of G4 amounts, decreasing from > 8 days in the south to < 5 days in the north (Fig. 9b). The distribution trend of G4 days is in accordance with the amounts, but the magnitude is relatively small. Both G4 amounts and days show a significant decreasing trend over the whole region (slightly more obvious than G3), with rates of −1.1 mm/decade and − 0.2 days/decade, respectively (Fig. 9c). The annual average G4 light precipitation amounts are generally the same as those of G2 and G3.

The proportion of G4 light precipitation amount shows a mixture of upward and downward trends over the study period (Fig. 9d), but only two stations pass the 0.05 significance level with decreasing trends. Conversely, the proportion of G4 light precipitation days gently increases (Fig. 9e). G4 day proportions increase to much greater extent than G4 amounts in the entire region (Fig. 9f). The annual average proportion of G4 light precipitation amount is generally the same as G2 and G3, but there were even fewer G4 days than G2 or G3 over the observation period.

Fig. 10a and b show the spatial distribution characteristics of G5

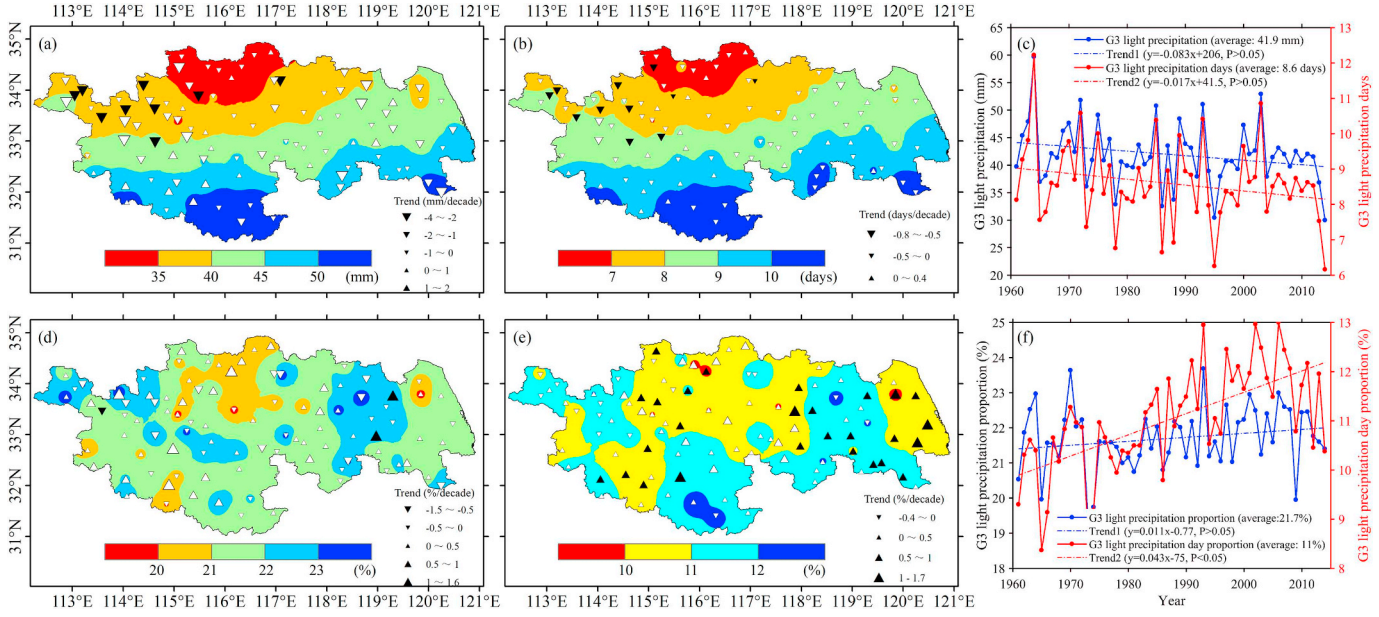

Fig. 8. The same as Fig. 6, but for G3 light precipitation events.

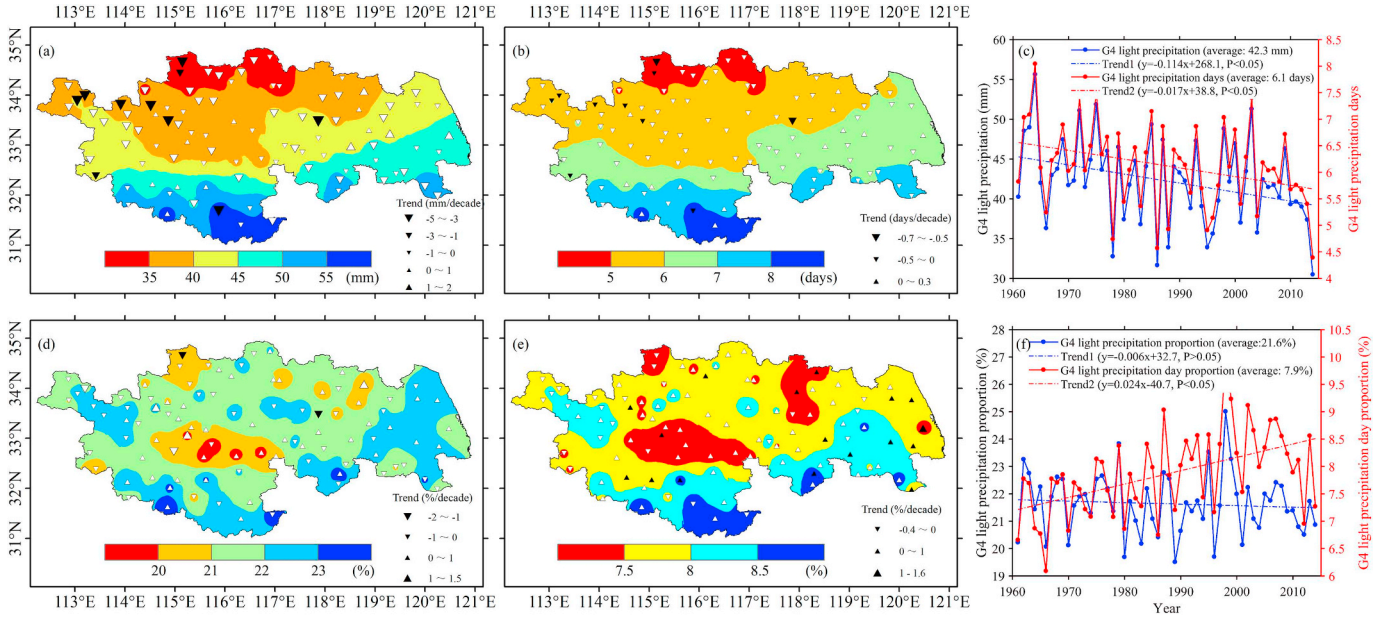

Fig. 9. The same as Fig. 6, but for G4 light precipitation events.

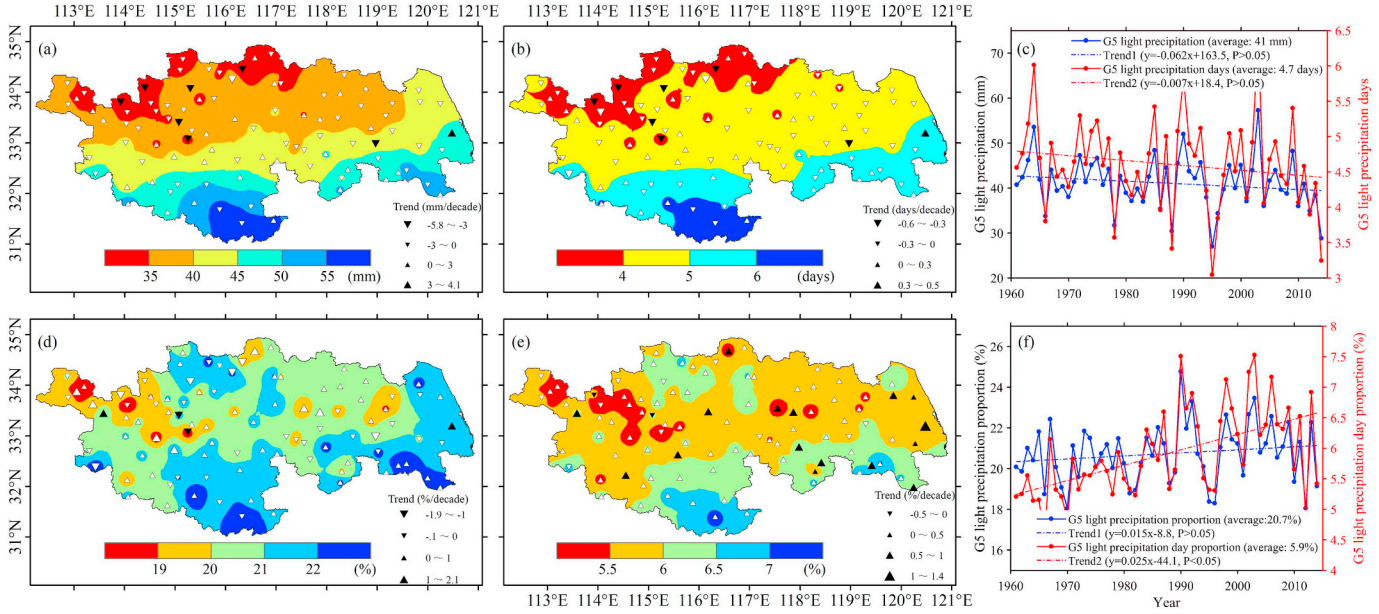

Fig. 10. The same as Fig. 6, but for G5 light precipitation events.

light precipitation amounts and days. The patterns are consistent with those of G4. Most stations exhibit a slight decreasing trend; only six stations in the northwestern parts of the region pass the 0.05 significance level. Both G5 light precipitation amounts and days slightly decrease (not significantly) over the whole region, but their magnitudes of interannual variations are large (Fig. 10c). The annual average G5 light precipitation amounts and days are roughly the same as those of the G4.

The proportions of G5 light precipitation amounts and days show both upward and downward trends (Fig. 10d, e). More stations pass the 0.05 significance test for G5 day proportions than amount proportions – in fact, stations tended to significantly increase in G5 day proportions. As shown in Fig. 10f, the proportions of G5 amounts slightly increase over the whole region while the proportion of G5 days increases significantly. The overall annual average proportions of G5 light precipitation amounts are generally similar to G2, G3, and G4, but there are even fewer G5 days than G2, G3, and G4.

Fig. 11 shows trends in the five grades of light precipitation events and their respective percentages of total light precipitation. As shown in Fig. 11a, G1 produces the least amount of precipitation (28.5 mm) but covers the most days (45.4 days). The precipitation amounts of G2, G3, G4, and G5 are similar (around 40 mm), but the number of precipitation days decreases from G1 to G5. G1 has the least amount of rainfall, but falls over the greatest number of days. The number of precipitation days decreases from G1 to G5 and at a particularly steep slope from G1 to G2. Among the five grades of light precipitation events, the decrease in G1 amounts and days was largest (over 0.05 significance). According to Fig. 11b, G1 occupied only 15.1% of the proportion of total light precipitation amounts, but more than half of the total light precipitation days. G1 events decreased significantly in terms of both precipitation amount and day count. In short, the overall decrease in light precipitation over the study period in HREC can be mainly attributed to G1.

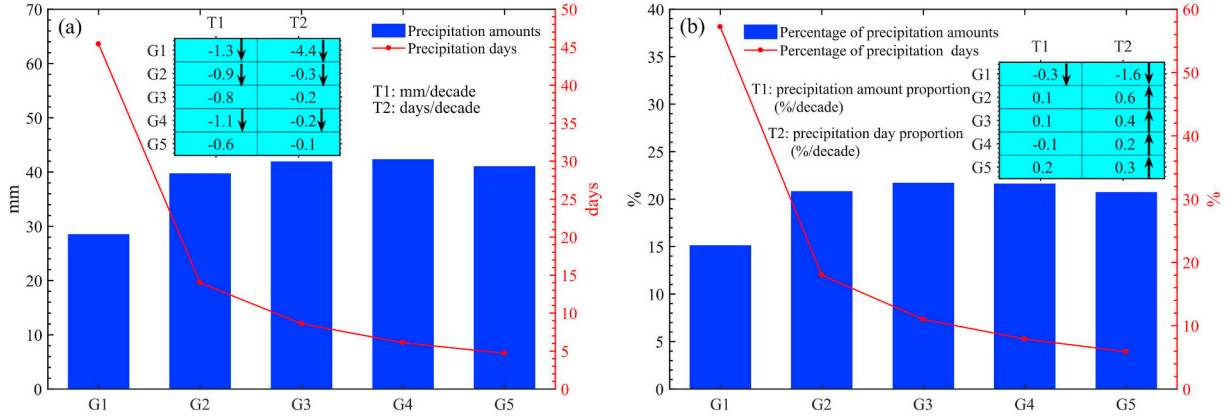

Fig. 11. Averages (1961–2014) of different levels of (a) light precipitation amounts and days, and (b) their percentages in total light precipitation. Table inside graph shows trends, where arrows represent linear trends reaching 0.05 significance level.

3.3. Consecutive light precipitation event trends

Few previous researchers have investigated consecutive light precipitation events, so we sought in this study to determine whether they present a significant downward trend in the HREC. As shown in Fig. 12a, consecutive light precipitation events across the region have a pronounced north-south gradient. The annual mean events across most southernmost parts of the region are > 10; most stations show a significant decreasing trend in consecutive light precipitation events. Fig. 12b shows the CvM statistics for consecutive light precipitation events during 1961–2014. The maximum divergence (statistical value of y-axes) occurs between 1977 and 1978, indicating substantial departure of the consecutive light precipitation events before and after the red line in Fig. 12b. The average value during 1978–2014 is significantly lower than that in 1961–1977 (Fig. 12c). The entire region shows a downward trend at rate of −1 events/decade from 1961 to 2014.

The southernmost part of the study area received about twice the amount of annual mean consecutive light precipitation as the northernmost (Fig. 12d). Consecutive light precipitation amounts appear to decrease significantly across the whole region at rates of −16 to −5 mm/decade. A significant change point was detected in 1977/1978 (Fig. 12e), with a mean of 81.9 mm/year in the earlier period (1961–1977) and a mean of 56 mm/year in the later period (1978–2014) (Fig. 12f). The entire study period showed a significant decreasing trend (−7.4 mm/decade) in annual consecutive light precipitation amounts.

The distribution of consecutive light precipitation days on the annual mean is similar to that of consecutive light precipitation amounts and events, decreasing from > 40 days in the south to < 20 days in the north (Fig. 12g). Almost the entire region shows a consistent downward trend. The number of annual consecutive light precipitation days abruptly changes in 1977 (Fig. 12h); the mean value of the later period is significantly lower than that of the earlier period (Fig. 12i). The regional average consecutive light precipitation days drop down to −4.1 days/decade.

The spatial distribution characteristics of the CLPMI are similar to those of consecutive light precipitation event frequency, amount, and day count (Fig. 12j). This is because the index is calculated based on the three variables. There are also spatially consistent decreasing trends in annual CLPMI. The mutation point of annual CLPMI emerges in 1977/1978 (Fig. 12k), and the average of the later period is 23.1 lower than that of the earlier period (Fig. 12l). The regional average annual CLPMI also shows a significant downward trend.

We calculated the differences in consecutive light precipitation events, amounts, days, and CLPMI between 1978–2014 to 1961–1978 (i.e., the average values of the period 1978–2014 minus the those of the period 1961–1977) to observe the spatial characteristics of consecutive light precipitation events before and after the mutation. As shown in Fig. 13a, the mean difference of consecutive light precipitation events between 1978–2014 and 1961–1977 indicates that the values in the eastern regions (approximately −12 events) are significantly smaller than other regions. As shown in Fig. 13b, the lowest values (approximately −50 mm) of consecutive precipitation amounts lie in the eastern parts of the region. The greatest differences (the values lower than −40 days) in consecutive light precipitation days appear to occur in the eastern parts of the region (Fig. 13c). Similarly, the minimum CLPMI values appear in the eastern parts of the region (Fig. 13d). In general, the mean differences in consecutive light precipitation events, amounts, days, and CLPMI have similar spatial distribution characteristics. Most stations passed the 0.05 significance test, which once again proves that the mean values of the later period (1978–2014) are significantly lower than that of the earlier period (1961–1977), especially in eastern parts of the region.

3.4. Possible mechanisms for decreasing trends in light precipitation events

G1 light precipitation shows the most obvious downward trend and the largest proportion of total light precipitation events among the five grades, so we choose a G1 event to analyze the possible mechanisms of light precipitation in the region. We consider a “light precipitation event” to have occurred in the study area when the number of stations experiencing G1 light precipitation in the same day is greater than one-third of the total number of stations. There are a total of 2567 days in the 54-year record (1961–2014). Fig. 14a shows that the G1 light precipitation days significantly decreased at a rate of −4.8 days/decade over this period. This trend is broadly consistent with the G1 light precipitation days shown in Fig. 6c, although the graphs were drawn using different statistical methods. According to Fig. 14b, we found that G1 light precipitation occurred least frequently in August; the most frequent occurrences were in May. The proportion of stations with G1 events in June–August is small, indicating that summer light precipitation has a certain regional locality. G1 coverage in February–May and September–November is high, indicating spring and autumn light precipitation events occur in a large extent over the HREC.

We explored light precipitation event mechanisms in this study using atmospheric circulation data. We focused on circulation characteristics corresponding to G1 light precipitation days. Fig. 15 shows vertically integrated water vapor transport anomalies during G1 light precipitation days for the period 1961–2010. The HREC is strongly influenced by the prevailing northerly water vapor transport anomalies during G1 days (Fig. 15a), indicating that this region is more prone to light precipitation events during the winter half of the year. The regional water vapor budgets significantly decrease (Fig. 15b) in

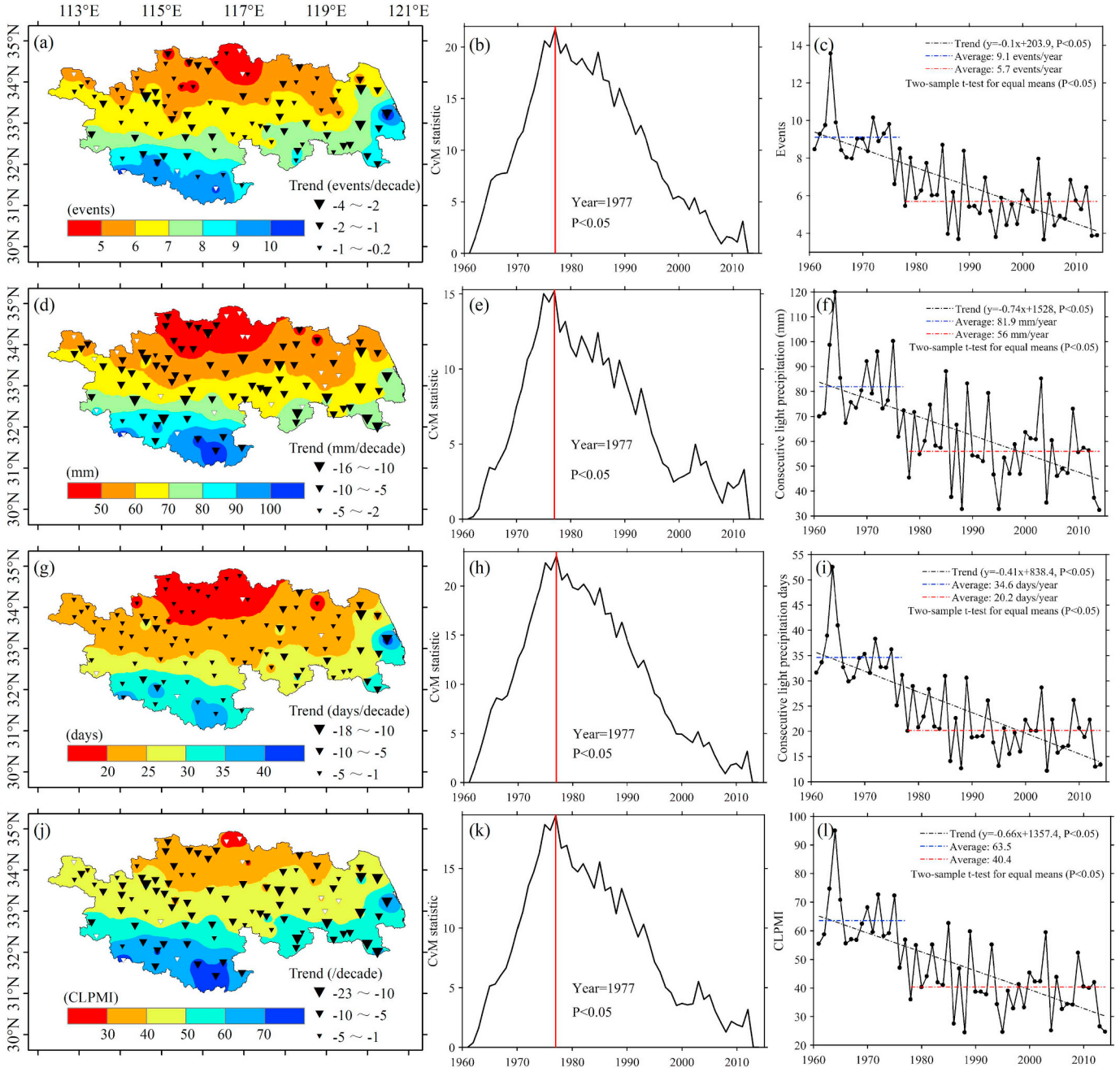

Fig. 12. Changes in consecutive light precipitation events. Panels (a-c) show consecutive light precipitation event spatial patterns, abrupt changes, and temporal characteristics. Panels (d-f) show consecutive light precipitation amount spatial patterns, abrupt changes, and temporal characteristics. Panels (g-i) show consecutive light precipitation day spatial patterns, abrupt changes, and temporal characteristics. Panels (j-l) show CLPMI spatial patterns, abrupt changes, and temporal characteristics. Solid triangles represent linear trends reaching 0.05 significance level.

accordance with the G1 trends discussed above (correlation coefficient reached 0.44). This indicates that a decrease in net water vapor transport creates a reduction in light precipitation events. Greater water vapor flux divergence values indicate low precipitation. As shown in Fig. 15b, water vapor flux divergence anomalies significantly increase (correlation coefficient is −0.40), indicating that elevated water vapor flux divergence in this region is responsible for a reduction in light precipitation events.

Cloud cover distribution characteristics also have important effects on the light precipitation events (Wu et al., 2017). We used annual cumulative low cloud cover and total column cloud liquid water data corresponding to G1 light precipitation days to explore the mechanism of G1 events. As shown in Fig. 16a, the HREC has a clear positive regression coefficient, indicating that low cloud cover makes positive contribution to light precipitation events. A decrease in low cloud cover leads to a reduction in light precipitation events. The annual accumulated low cloud cover on G1 light precipitation days decreases on the whole, which decreases light precipitation events. The regression patterns for total column cloud liquid water (Fig. 16b) also suggest a positive contribution of total column cloud liquid water to light precipitation events. Downward trends in total column cloud liquid water appear to be closely related to the decreasing trends in light precipitation events.

We used linear regression analysis to explore the possible linkages between air temperature and light precipitation events. The pressure-longitude cross section of the zonal temperature analysis shows a

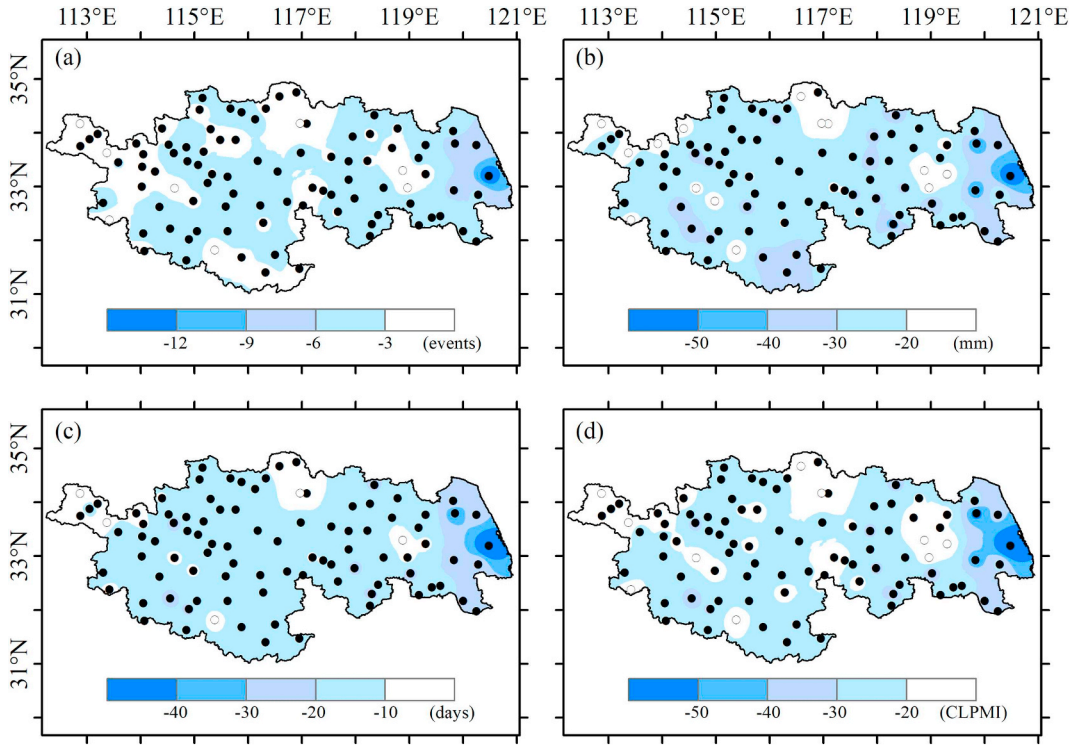

Fig. 13. Mean differences of consecutive light precipitation (a) events, (b) amounts, (c) days and (d) CLPMI between 1978–2014 and 1961–1977. Black dots denote areas passing 0.05 significance level, white dots represent regions not passing 0.05 significance level.

negative correlation between temperature and light precipitation events, implying that the rising temperature is not conducive to the formation of light precipitation (Fig. 17a). Warming in the middle and lower troposphere is greater than that in the near surface. According to Fig. 17b, the regression coefficient of meridional air temperature is also negative over the HREC (31°-35°N), indicating that higher temperatures correspond to less light rain. The warming gradient of the meridional temperature in the lower troposphere is not as obvious as that of zonal temperature over the study area.

The vertical movement of the atmosphere plays an important role in the formation of precipitation (Karki et al., 2018). We analyzed the annual vertical velocity field during G1 light precipitation days. According to the pressure-longitude cross section of the zonal vertical velocity averaged over 31°-35°N regressed onto G1 days (Fig. 18a), there is upward convective motion over most of the HREC (112°-118°E) in the lower troposphere. The vertical velocity values show upward trends in the lower troposphere over most of the study area, indicating that weakening upward motion causes a reduction in light precipitation events. As shown in Fig. 18b, negative correlations exist between vertical velocity and light precipitation events in the lower troposphere of the study area (31°–35°N); in effect, larger upward motion results in fewer light precipitation events. The vertical velocity of the lower troposphere also trends upward, indicating weaker upward motion again accompanied by a reduction in light precipitation events.

4. Discussion

We observed no obvious trend in annual precipitation amount over the study period, but the number of precipitation days appears to have significantly decreased trend in the HREC. Similar results were found by Zhai et al. (2005), who pointed out that the number of precipitation days has decreased significantly in eastern China. The number of light precipitation days accounts for 75.7% of the total precipitation days in the HREC, so we infer that the decrease in precipitation day count is

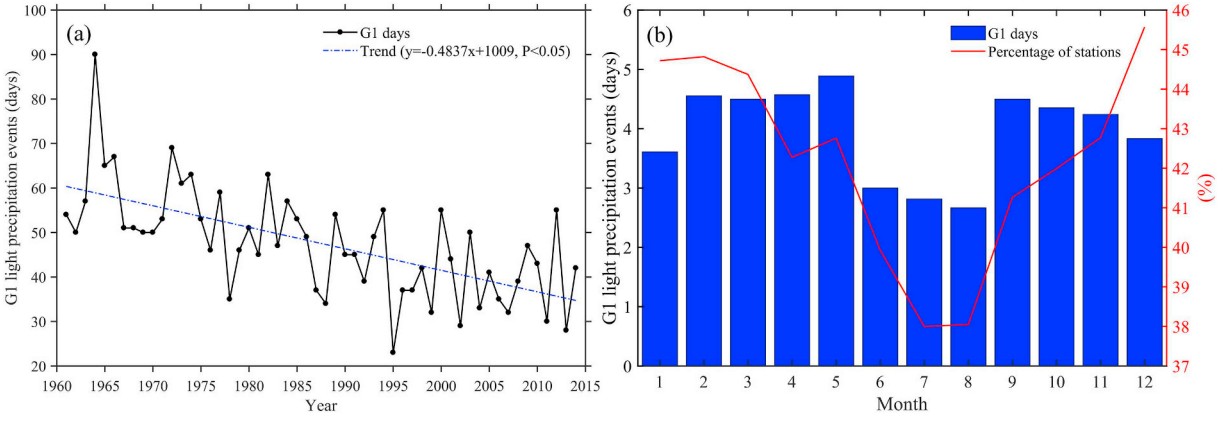

Fig. 14. Occurrence of (a) G1 light precipitation events and (b) number of G1 days during each month over HREC.

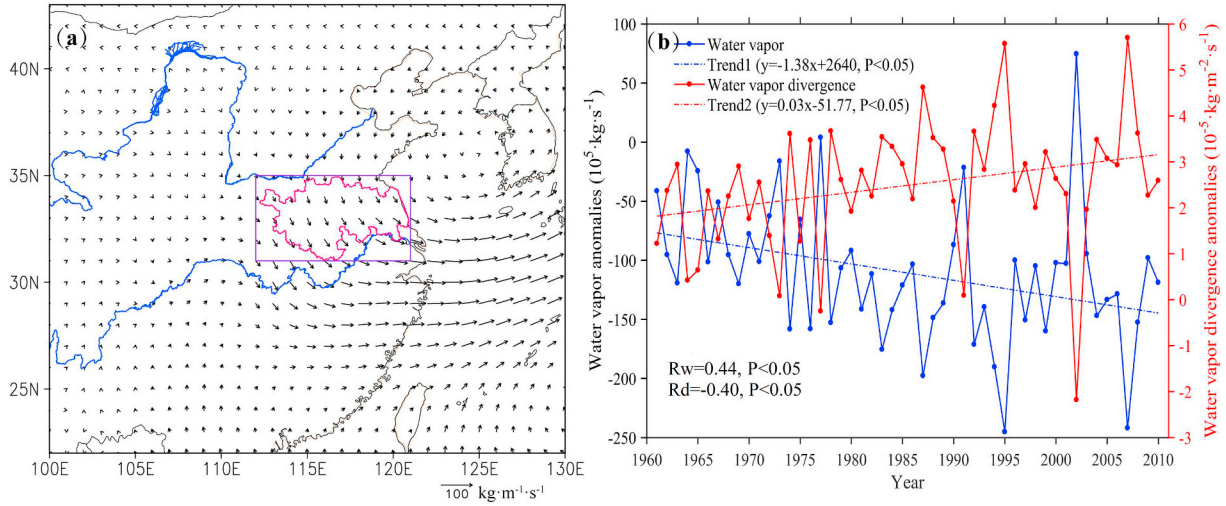

Fig. 15. (a) Annual average (1961–2010) water vapor transport anomalies and (b) annual series of net water vapor transport anomalies and divergence anomalies at vertically integrated layer (surface to 300 hPa) during G1 light precipitation days over HREC. Modena box (112°-121°E, 31°-35°N) quantifies net water vapor transport anomalies and divergence across four boundaries. Rw represents correlation between net water vapor transport anomalies and G1 days. Rd denotes correlation between net water vapor transport divergence anomalies and G1 days.

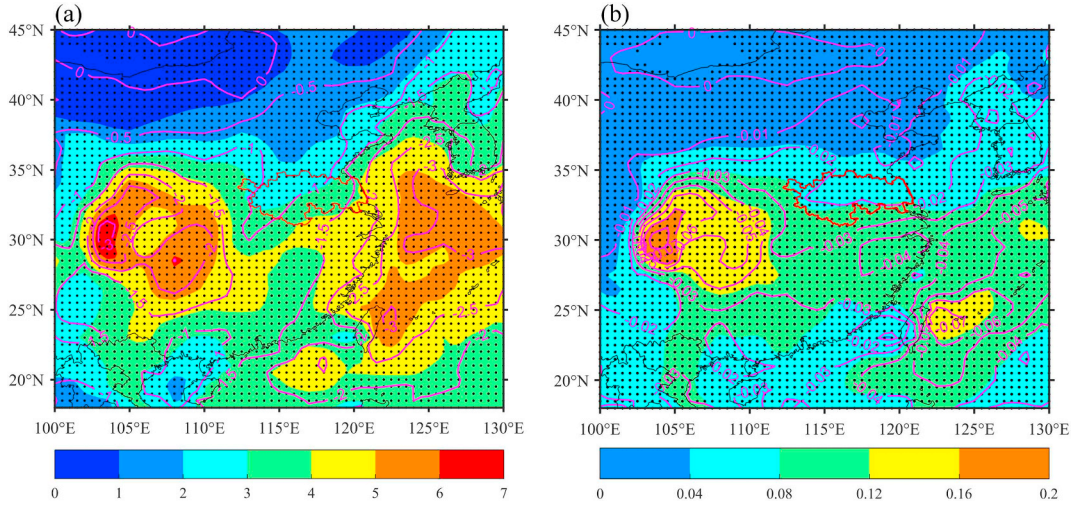

Fig. 16. (a) Regression patterns (shaded, tenths) of low cloud cover onto number of G1 days. The day variation of low cloud cover varies from 0 to 10 tenths. Regions with black dots indicate regression coefficients passing 0.05 significance level. Purple-red contour indicates trends (tenths·day·year^{-1}) in accumulated low cloud amount on annual G1 days. (b) Regression patterns (shaded, kg·m^{-2}) of total column liquid water onto number of G1 days. Purple-red contour indicates trends (kg·m^{-2}·day·year^{-1}) in accumulated total column liquid water on annual G1 days. (For interpretation of the references to colour in this figure legend, the reader is referred to the web version of this article.)

mainly due to the significant decrease in the number of light precipitation days. Taken together, our results suggest that precipitation events in the HREC are growing continually more intense, yet less frequent.

We next calculated precipitation frequency (number of days) at different intensity levels during two equal time periods, that is 1961–1987 and 1988–2014. As shown in Fig. 19, there are significantly fewer light precipitation days in the later period (1988–2014) than the earlier period (1961–1987), though the number of heavy precipitation days in the later period exceeds that of the earlier period. Fig. 19 indicates that heavy precipitation (i.e., extreme events) have become more frequent at the expense of a decrease in light precipitation in the HREC. Previous researchers have made similar results (Fischer and Knutti, 2016). Heavy precipitation releases a great deal of latent heat which offsets energy perturbations and consumes a large amount of water vapor in the atmosphere, thus driving down the likelihood of light precipitation events (Allen and Ingram, 2002; Wu et al., 2015).

We set $0.1 \le P < 10$ mm/day as the light precipitation event threshold and compared our results to those of previous studies (Qian et al., 2007; Qian et al., 2010; Wu et al., 2017). Again, we observed a significant decrease in annual light precipitation amounts and days in the HREC. The standard of $0.1 \le P < 10$ mm/day does not reveal detailed variations in light precipitation, so we divided the criterion into five light precipitation grades as discussed in detail above – we found that downward trends in G1 ($0.1 \le P < 2$ mm/day) light precipitation amounts and days are more obvious than other grades. As the intensity of light precipitation increases, the downward trend in specific events is less obvious. The G1 proportion of total light precipitation in small (15.1%), but the number of G1 days accounts for more than half of the total light precipitation days. Accordingly, it is more reasonable to use $0.1 \le P < 2$ mm/day as the standard for light precipitation events in the HREC. Previous researchers have used a similar standard to find that decrease in precipitation events is mainly concentrated at lower light precipitation intensities (Liu et al., 2011; Qian et al., 2009).

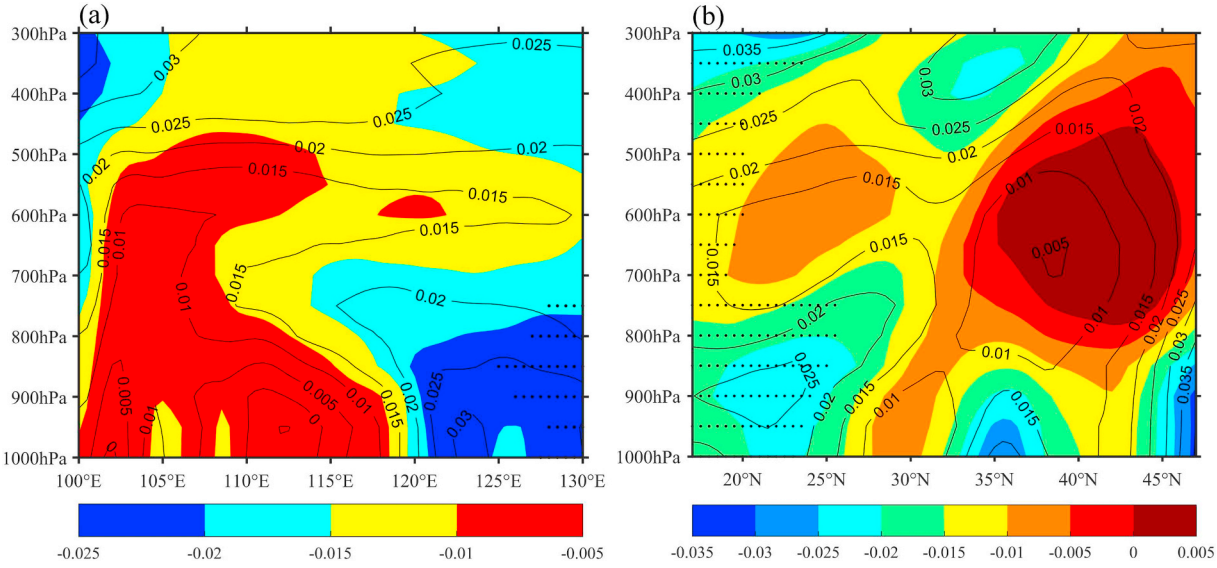

Fig. 17. (a) Regression patterns of zonal air temperature (shaded, ˚C) averaged over 31˚-35˚N onto number of G1 days. Regions with black dots indicate regression coefficients passing 0.05 significance level. Black contour indicates trends (˚C·year^{-1}) in air temperature on the annual G1 light precipitation days. (b) Regression patterns of meridional air temperature (shaded, ˚C) averaged over 112˚-121˚E onto number of G1 days.

The light precipitation event is discrete; it does show a significant downward trend, but it is necessary to determine whether consecutive events are decreasing on the whole. We defined a duration ≥3 consecutive days with daily variable values above the specific threshold as a "consecutive event", as previous scholars have also done (Nastos and Zerefos, 2009; Ren et al., 2013; Russo et al., 2015; Singh et al., 2014). We found that the events (frequency) and CLPMI of consecutive light precipitation significantly decreases over the observation period in the HREC. The amounts and days of consecutive light precipitation events decrease to greater extent than discrete light precipitation events. An increase in consecutive extreme events (e.g., prolonged dry spells and consecutive precipitation extremes) appears to come at the expense of a reduction in consecutive light precipitation events. The events (frequency), amounts, number of days, and CLPMI of consecutive light precipitation changed significantly in 1977/1978 over the entire HREC; mean values of the later period are significantly lower than those of the earlier period. This point of mutation is consistent with the abrupt change in the low-intensity light precipitation events in the literature (Liu et al., 2011). This may be due to other climatic phenomena such as abrupt reductions in solar radiation, total cloud cover, and surface air pressure in 1977/1978 (Kaiser, 2000; Liang and Xia, 2005).

We find that light precipitation events are least common during the summer (June–August), during which time water vapor is abundant and the vertical movement of the atmosphere is very strong which is conducive to the occurrence of extreme precipitation events rather than light rain (Li et al., 2016; Zhang et al., 2017). Researchers tend to monthly atmospheric variables to explain decreasing light precipitation event trends. Monthly average atmospheric circulation variables, which include non-light precipitation days, may contain considerable uncertainty. For example, Qian et al. (2009) found weak correlation

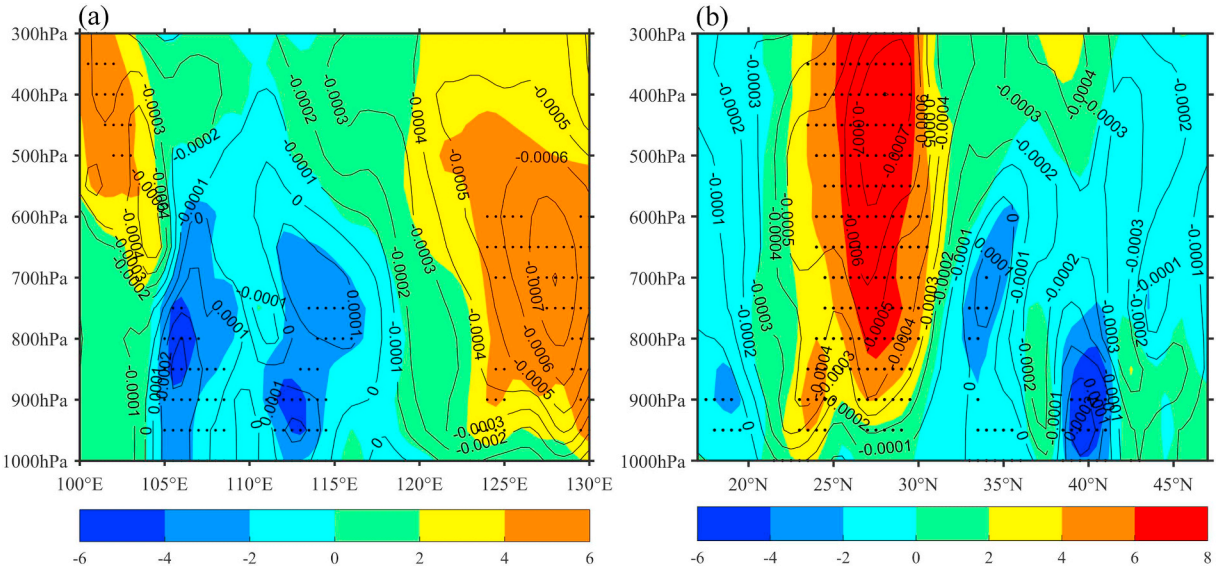

Fig. 18. (a) Regression patterns of zonal vertical velocity (shaded, negative values indicate upward motion, 10^{-4} Pa·s^{-1}) averaged over 31˚-35˚N onto number of G1 days. Regions with black dots indicate regression coefficients passing 0.05 significance level. Black contour indicates trends (Pa·s^{-1}·year^{-1}) of vertical velocity on annual G1 days. (b) Regression patterns of meridional vertical velocity (shaded, negative values indicate upward motion, 10^{-4} Pa·s^{-1}) averaged over 112˚-121˚E onto number of G1 days.

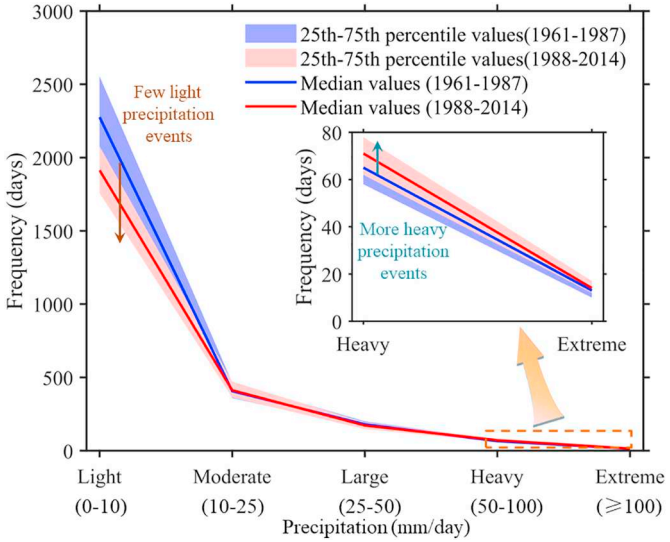

Fig. 19. Changes in precipitation distribution over 1961–1987 versus 1988–2014.

between light precipitation events and large-scale water vapor transport using a monthly water vapor transport mean, which does not accord with our results. We investigated the vertically integrated water vapor transport budgets corresponding to G1 light precipitation days and found closely consistent trends among water vapor and light precipitation indices. Wu et al. (2015) reached similar results using composite analysis for light precipitation days and lower-tropospheric water content. Trends in light precipitation events appear to be closely related to changes in water vapor transport in the HREC.

We also conducted a linear regression analysis between low cloud cover, total column cloud liquid water, and G1 light precipitation days. The regression values are significantly positive in the HREC, which suggests that a decrease in low cloud cover and total column cloud liquid water may be responsible for the reduction in light precipitation events over the study period. This result is in accordance with the results of previous studies (Liu et al., 2011; Wu et al., 2017; Wu et al., 2015). The rate at which air temperature increases in the middle and lower troposphere is greater than that in the near surface in the HREC, which indicates that reduction in light precipitation events is accompanied by increasing temperature. Given a relatively stable level of water vapor content in the lower troposphere, it is harder than usual for warmer air to reach the dew-point temperature, thus resulting in a decrease in trace and light precipitation events (Qian et al., 2007; Wu et al., 2015).

We also found that vertical upward motion has weakened in the HREC to a critical degree, which is also likely responsible for the reduction in light precipitation events over the region. Based on the vertical motion mechanism, Wen et al. (2016) designed an atmospheric static stability index that reflects variations in precipitation intensity; they found that some light precipitation events have become relatively heavier precipitation events and that the number of light precipitation days has decreased correspondingly over East China. It is possible that the weakening of static stability has caused increases in precipitation intensity by increasing upward motion, and vice versa.

In addition to circulation, atmospheric aerosol content also markedly affects the intensity and duration of light precipitation events. Recent researchers have attributed the reduction in light precipitation events to an increase in aerosol concentration (Qian et al., 2009; Wu et al., 2016; Zhao et al., 2006). Aerosols may significantly increase droplet quantity and reduce droplet size, which suppresses light precipitation (Gong et al., 2007). However, the temporal length of aerosol data (observations or simulations) used in these studies is relatively short, and the effects of aerosol usage on light precipitation merits further study based on long-term data.

5. Conclusions

Although light precipitation amount accounts for only 22.5% of the total precipitation in the HREC, the number of light precipitation days ($0.1 \le P < 10$ mm/day) accounts for 75.7% of the total precipitation days. To this effect, light precipitation events are crucial indicators of climate change in the HREC, which belongs to a climate transitional zone. In this study, we investigated the spatial and temporal characteristics of light precipitation events and explored their mechanisms as-associated with a series of atmospheric variables. Our most notable conclusions can be summarized as follows:

(1) The distribution of light precipitation amounts and days decreased from south to north with distinct zonal distribution features. The number of light precipitation days has decreased to greater extent than the amount of light precipitation in the HREC. The number of G1 days accounts for 57.2% of the total light precipitation days; decreasing light precipitation trends can be attributed to changes in G1 events ($0.1 \le P < 2$ mm/day). This is because the decreasing trends in G1 light precipitation amounts and days are more obvious than other levels of the light precipitation events.
(2) Consecutive light precipitation events across the region show a pronounced north-south gradient in the HREC. The frequency, amounts, days and CLPMI of consecutive light precipitation events decreased significantly from 1961 to 2014, and the mean value of the latter period (1978–2014) is significantly lower than that of the earlier period (1961–1977). Consecutive light precipitation events appear to be more sensitive than discrete light precipitation events and have decreased to greater extent in the study region.
(3) According to atmospheric circulation variables corresponding to G1 days, there is obvious positive correlation between water vapor transport budgets, low cloud cover, total column cloud liquid water content and light precipitation events. The relationships between water vapor flux divergence and light precipitation events, between air temperature and light precipitation events, and between vertical velocity and light precipitation events all show significant negative correlations. Decreases in water vapor transport budgets, low cloud cover, and total column cloud liquid water may be responsible for the HREC's reduction in light precipitation events. Increases in water vapor flux divergence, air temperature, and vertical velocity values also may have caused a reduction in light precipitation events.

Acknowledgements

This study is supported by the Open Project of Huai River Eco-economic Corridor Research Institute (HHKF201909), the MOE (Ministry of Education in China) Project of Humanities and Social Sciences (19YJCZH259), National Key Research and Development Program of China (2016YFA0601700), the National Natural Science Foundation of China (41471425), and the Huai'an Xiangyu Talent Foundation (31ZYQ01).

References

Ahmed, K., Shahid, S., Nawaz, N., 2018. Impacts of climate variability and change on seasonal drought characteristics of Pakistan. Atmos. Res. 214, 364–374.
Ahmed, K., Shahid, S., Chung, E.-S., Wang, X.-j., Harun, S.B., 2019. Climate change uncertainties in seasonal drought severity-area-frequency curves: case of arid region of Pakistan. J. Hydrol. 570, 473–485.
Allen, M.R., Ingram, W., 2002. Constraints on future changes in climate and the hydrologic cycle. Nature 419, 224–232.
Dai, A., 2013. Increasing drought under global warming in observations and models. Nat. Clim. Chang. 3 (1), 52–58.
Dhana Lakshmi, D., Satyanarayana, A.N.V., 2019. Influence of atmospheric rivers in the

occurrence of devastating flood associated with extreme precipitation events over Chennai using different reanalysis data sets. Atmos. Res. 215, 12–36.
Duan, A., Wu, G., 2008. Weakening trend in the atmospheric heat source over the Tibetan Plateau during recent decades. Part I: observations. J. Clim. 21 (13), 3149–3164.
Fischer, E.M., Knutti, R., 2016. Observed heavy precipitation increase confirms theory and early models. Nat. Clim. Chang. 6 (11), 986–992.
Fu, J., Qian, W., Lin, X., Chen, D., 2008. Trends in graded precipitation in China from 1961 to 2000. Adv. Atmos. Sci. 25 (2), 267–278.
Gao, M., Mo, D., Wu, X., 2016. Nonstationary modeling of extreme precipitation in China. Atmos. Res. 182, 1–9.
Gong, D.Y., et al., 2007. Weekly cycle of aerosol-meteorology interaction over China. J. Geophys. Res.: Atmos. 112, D22202.
Gu, W., Zhang, P., 2016. A study of the planning and development of the Huaihe bio-economic zone. J. Jiangsu Univ. (Soc. Sci. Ed.) 18 (1), 19–23 (in Chinese).
Holmes, M., Kojadinovic, I., Quessy, J.F., 2013. Nonparametric tests for change-point detection à la Gombay and Horváth. J. Multivar. Anal. 115 (115), 16–32.
IPCC, 2013. Climate Change 2013: The Physical Science Basic. Contribution of Working Group I to the Fifth Assessment Report of the Intergovernmental Panel on Climate Change. Cambridge University Press, Cambridge, United Kingdom and NewYork, USA.
Kaiser, D.P., 2000. Decreasing cloudiness over China: an updated analysis examining additional variables. Geophys. Res. Lett. 27 (15), 2193–2196.
Karki, R., et al., 2018. WRF-based simulation of an extreme precipitation event over the Central Himalayas: Atmospheric mechanisms and their representation by micro-physics parameterization schemes. Atmos. Res. 214, 21–35.
Li, L., Li, W., Tang, Q., Zhang, P., Liu, Y., 2016. Warm season heavy rainfall events over the Huaihe River Valley and their linkage with wintertime thermal condition of the tropical oceans. Clim. Dyn. 46 (1–2), 71–82.
Liang, F., Xia, X.A., 2005. Long-term trends in solar radiation and the associated climatic factors over China for 1961-2000. Ann. Geophys. 23 (7), 2425–2432.
Lin, H., You, Q., Zhang, Y., Jiao, Y., Fraedrich, K., 2016. Impact of large-scale circulation on the water vapour balance of the Tibetan Plateau in summer. Int. J. Climatol. 36, 4213–4221.
Liu, B., Xu, M., Henderson, M., 2011. Where have all the showers gone? Regional declines in light precipitation events in China, 1960–2000. Int. J. Climatol. 31 (8), 1177–1191.
Mallakpour, I., Villarini, G., 2015. The changing nature of flooding across the Central United States. Nat. Clim. Chang. 5 (3), 250–254.
Mazdiyasni, O., Aghakouchak, A., 2015. Substantial increase in concurrent droughts and heatwaves in the United States. Proc. Natl. Acad. Sci. U. S. A. 112 (37), 11484–11489.
Nastos, P.T., Zerefos, C.S., 2009. Spatial and temporal variability of consecutive dry and wet days in Greece. Atmos. Res. 94 (4), 616–628.
Poli, P., et al., 2013. The Data Assimilation System and Initial Performance Evaluation of the ECMWF Pilot Reanalysis of the 20th-Century Assimilating Surface Observations Only (ERA-20C). European Centre for Medium Range Weather Forecasts, Reading.
Qian, W., Fu, J., Yan, Z., 2007. Decrease of light rain events in summer associated with a warming environment in China during 1961–2005. Geophys. Res. Lett. 34 (11), 224–238.
Qian, Y., et al., 2009. Heavy pollution suppresses light rain in China: Observations and modeling. J. Geophys. Res. Atmos. 114 (D7), D00K02.
Qian, Y., Gong, D., Leung, R., 2010. Light rain events change over North America, Europe, and Asia for 1973-2009. Atmos. Sci. Lett. 11 (4), 301–306.
Ren, X., Yang, X.Q., Sun, X., 2013. Zonal oscillation of western pacific subtropical high and subseasonal SST Variations during Yangtze Persistent Heavy Rainfall events. J. Clim. 26 (22), 8929–8946.
Russo, S., et al., 2015. Magnitude of extreme heat waves in present climate and their projection in a warming world. J. Geophys. Res. Atmos. 119 (22), 12,500–12,512.
Sharma, S., Mujumdar, P., 2017. Increasing frequency and spatial extent of concurrent meteorological droughts and heatwaves in India. Sci. Rep. 7, 15582.
Singh, D., Tsiang, M., Rajaratnam, B., Diffenbaugh, N.S., 2014. Observed changes in extreme wet and dry spells during the South Asian summer monsoon season. Nat. Clim. Chang. 4 (6), 456–461.
Tao, H., Borth, H., Fraedrich, K., Schneidereit, A., Zhu, X., 2016. Hydrological extremes in the Aksu-Tarim River Basin: Climatology and regime shift. Clim. Dyn. 46 (7–8), 2029–2037.
Trenberth, K.E., 1991. Climate diagnostics from global analyses: conservation of mass in ECMWF analyses. J. Clim. 4 (7), 707–722.
Wang, X., Hou, X., Wang, Y., 2017. Spatiotemporal variations and regional differences of extreme precipitation events in the Coastal area of China from 1961 to 2014. Atmos. Res. 197, 94–104.
Wen, G., Huang, G., Tao, W., Liu, C., 2016. Observed trends in light precipitation events over global land during 1961–2010. Theor. Appl. Climatol. 125 (1–2), 161–173.
Wu, J., Zhang, L., Zhao, D., Tang, J., 2015. Impacts of warming and water vapor content on the decrease in light rain days during the warm season over eastern China. Clim. Dyn. 45 (7–8), 1841–1857.
Wu, J., Ling, C., Zhao, D., Zhao, B., 2016. A counterexample of aerosol suppressing light rain in Southwest China during 1951–2011. Atmos. Sci. Lett. 17 (9), 487–491.
Wu, J., et al., 2017. Impacts of cloud cover on long-term changes in light rain in Eastern China. Int. J. Climatol. 37 (12), 4409–4416.
Yao, H., Li, D., Wang, H., 2017. A comparative analysis of the atmospheric circulation in summertime rainy days with different precipitation intensity in eastern Northwest China during 1981-2012. Acta Meteorologica Sinica 75 (3), 384–399 (in Chinese).
Yu, H., Wang, L., Yang, R., Yang, M., Gao, R., 2018. Temporal and spatial variation of precipitation in the Hengduan Mountains region in China and its relationship with elevation and latitude. Atmos. Res. 213, 1–16.
Zhai, P., et al., 1999. Changes of climate extremes in China. Clim. Chang. 42 (1), 203–218.
Zhai, P., Zhang, X., Wan, H., Pan, X., 2005. Trends in total precipitation and frequency of daily precipitation extremes over China. J. Clim. 18 (7), 1096–1108.
Zhang, W., et al., 2015. Changes in extreme climate events in eastern China during 1960–2013: a case study of the Huaihe River Basin. Quat. Int. 380-381, 22–34.
Zhang, Y., You, Q., Ye, L., Chen, C., 2017. Spatio-temporal variability and possible mechanism of rainy season precipitation in Poyang Lake Basin, China. Clim. Res. 72, 129–140.
Zhao, C., Tie, X., Lin, Y., 2006. A possible positive feedback of reduction of precipitation and increase in aerosols over eastern central China. Geophys. Res. Lett. 33 (11), L11814.
Zhou, T., 2003. Comparison of the global air-sea freshwater exchange evaluated from independent datasets. Prog. Nat. Sci. 13 (8), 626–631.